Stochastic methods in damage detection

M. Oberguggenberger,[1*] and M. Schwarz[1]

[1] *Unit for Engineering Mathematics, University of Innsbruck, Austria*
[*] Corresponding author: michael.oberguggenberger@uibk.ac.at

Abstract

This paper reports on a new method for analyzing wave propagation in two- and three-dimensional random materials. The applicative targets are damage detection, system identification, and calibration of models for randomly perturbed structures. The novelty of the approach is that the dynamic response of the structure is represented by means of Fourier integral operators. Parameter calibration and identification as well as describing the random behavior is achieved through the coefficients in the Fourier integral operators. Damage detection proceeds in three steps: (a) calibration of the nominal material parameters at the undamaged, but possibly randomly perturbed structure; (b) calibration of the stochastic parameters of the random fields perturbing the material properties of the structure; (c) damage such as overall deviation of the nominal parameters or such as cracks are detected by finding the features of the dynamic response outside the confidence region computed from steps (a) and (b). The applicability of the method is demonstrated by means of computer simulations of an elastic body under plane strain.

Keywords: Waves in random media, Fourier integral operators, numerical simulation, parameter calibration, damage detection.

1 Introduction

The paper reports on the results of a research project[1] addressing linear wave propagation in random media by means of stochastic Fourier integral operators. The applicative targets are reliability analysis, damage detection, system identification, and calibration of models for randomly perturbed structures in elasticity and strength of materials. The set-up applies to materials with stochastically varying properties.

The dynamic response of an elastic medium is described by the equations of motion, a system of hyperbolic differential equations. Randomness of the medium causes the coefficients of the equations to become random fields. The direct, bottom-up approach would start by modelling the coefficients as random fields, solving the equations, and inferring stochastic properties of the solution. However, the direct approach faces the difficulty that the realizations of the random fields commonly in use in elastostatics do not have the degree of smoothness required to construct solutions in the propagation case. Thus the stochastic characteristics of the solutions are hardly tractable explicitly. Our approach consists in representing the dynamic response of the structure by means of stochastic Fourier integral operators and in shifting the stochastic modelling from the coefficients to stochastic building blocks of the Fourier integral operator.

A Fourier integral operator consists of a complex exponential term containing the phase function (which describes the propagation geometry) and an amplitude. In the linear, constant coefficient case, the response of the system can be expressed explicitly by means of Fourier integral operators based on so-called half wave equations. In the case of a spatially varying medium, we add parametrically described random terms to the phase function and amplitude of the Fourier integral operator, which carry the burden of modelling the random medium and can still be computed numerically. Since neither the stochastic models of the coefficients nor the ones of the phase function and amplitude are known a priori, but have to be determined by data fitting, our top-down approach appears as justified as the bottom-up approach. Parameter calibration is shifted to the terms constituting the Fourier integral operators and comparing the solution produced by the Fourier integral operator with measured data.

The paper starts with setting up the required theory: the equations of motion of three-dimensional linear elasticity, Fourier integral operators (FIOs) and the decomposition of scalar wave equations into two half wave equations, stochastic Fourier integral operators, numerical methods for evaluating the action of a Fourier integral operator, and the description of a two-dimensional test example.

The second part of the paper addresses the central theme of the project, namely stochastic parameter estimation and damage detection. The test runs are performed on data generated by a finite element

[1] Project No. 4602529, "Fourier Integral Operators in Stochastic Structural Analysis", Bridge Program, The Austrian Research Promotion Agency (FFG), together with INTALES Engineering Solutions, Natters, Austria, 2014 – 2017.

model (FEM), whereby the FE-output simulates measured data. The section starts with calibrating the nominal values of the material parameters and continues with calibrating the stochastic parameters of the underlying spatial random perturbations. Note that the Fourier integral operators have a deterministic part, in which the material properties, such as the modulus of elasticity, the Poisson ratio and the density, enter through the wave speed. Comparison of the FE-output with the solution produced by the FIO representation thus admits calibration of the nominal values. The stochastic part of the Fourier integral operator is modeled through a Gaussian random field with a correlation length and a variance to be determined. Assuming a sample of FE-data given in sufficiently many points, the correlation length can be estimated. Concerning the variances, it turned out that the variance of the random field applied in the FE-model does not coincide with the variance needed for the random fields in the Fourier integral operators. This obstacle was overcome by introducing a scaling curve which relates the two variances so that the FIO solution reproduces the stochastic properties of the FEM-solution. This scaling curve was obtained empirically by a large number of parameter variations and Monte Carlo simulations.

Finally, having calibrated the Fourier integral operator to the undamaged, but possibly randomly perturbed structure, this information can be used to produce confidence regions around undamaged solutions. With the help of these confidence regions, statistical tests can be set up that admit deciding about larger deviations in the overall material parameters as well as deciding about the presence of cracks. Using a grid of (virtual) sensors, the crack location can also be determined. This method works if the excitation source, the sensors, and the cracks are sufficiently close to each other. For larger scale distances, the FIOs have to be evaluated over a longer time period, which requires increasing numerical effort. Some of the results have been announced in [1, 2].

2 Theory

This section is devoted to collect the background material required for the methods employed. Starting with the equations of motion of linear elasticity, we turn to Fourier integral operators (FIOs) and the representation of the solution to scalar wave equations, followed by introducing stochastic terms in the FIOs and fast numerical methods for the evaluation of FIOs. The section concludes by presenting a plane strain test example to be used in Section 3.

2.1 Three dimensional linear elasticity

The dynamic displacement $\boldsymbol{u}(\boldsymbol{x},t)$ of a three-dimensional homogeneous, isotropic, linearly elastic body is given by the equations of motion

$$\frac{\lambda+\mu}{\rho}(\nabla\times\nabla\times\boldsymbol{u}(\boldsymbol{x},t))+\frac{\mu}{\rho}\Delta\boldsymbol{u}(\boldsymbol{x},t)-\partial_{tt}\boldsymbol{u}(\boldsymbol{x},t)=-\boldsymbol{f}(\boldsymbol{x},t), \tag{1}$$

where $\boldsymbol{f}$ is the body force, λ and μ are the Lamé constants and ρ the density. The lateral resp. the transverse wave speeds are $c_l^2=\frac{\lambda+2\mu}{\rho}$ resp. $c_s^2=\frac{\mu}{\rho}$. In this case, there exist [3, 4] potentials Φ and $\boldsymbol{\Psi}=(\Psi_1,\Psi_2,\Psi_3)^{\mathrm{T}}$ with

$$\begin{aligned}\nabla\Phi(\boldsymbol{x},t)+\nabla\times\boldsymbol{\Psi}(\boldsymbol{x},t)&=\boldsymbol{u}(\boldsymbol{x},t)\\ \nabla\cdot\boldsymbol{\Psi}(\boldsymbol{x},t)&=0,\end{aligned}$$

where Φ and $\boldsymbol{\Psi}$ satisfy the wave equations

$$\begin{aligned}\partial_{tt}\Phi(\boldsymbol{x},t)-c_l^2\Delta\Phi(\boldsymbol{x},t)&=-\varphi(\boldsymbol{x},t)\\ \partial_{tt}\Psi_j(\boldsymbol{x},t)-c_s^2\Delta\Psi_j(\boldsymbol{x},t)&=-\psi_j(\boldsymbol{x},t),\quad j=1,2,3,\end{aligned}$$

and φ and $\boldsymbol{\psi}$ have to be determined from

$$\begin{aligned}\nabla\varphi(\boldsymbol{x},t)+\nabla\times\boldsymbol{\psi}(\boldsymbol{x},t)&=-\boldsymbol{f}(\boldsymbol{x},t)\\ \nabla\cdot\boldsymbol{\psi}(\boldsymbol{x},t)&=0.\end{aligned}$$

In this way, the equations of motion (1) are decoupled into four scalar wave equations for the wave potentials. One can compute φ and $\boldsymbol{\psi}$ by inverting the Laplace equation as follows, using the ansatz

$$\begin{aligned}\varphi(\boldsymbol{x},t)&=\partial_x g_1(\boldsymbol{x},t)+\partial_y g_2(\boldsymbol{x},t)+\partial_z g_3(\boldsymbol{x},t)\\ \psi_1(\boldsymbol{x},t)&=\partial_z g_2(\boldsymbol{x},t)-\partial_y g_3(\boldsymbol{x},t)\\ \psi_2(\boldsymbol{x},t)&=-\partial_z g_1(\boldsymbol{x},t)+\partial_x g_3(\boldsymbol{x},t)\\ \psi_3(\boldsymbol{x},t)&=\partial_y g_1(\boldsymbol{x},t)-\partial_x g_2(\boldsymbol{x},t),\end{aligned}$$

for functions $g_j, j = 1, 2, 3$ to be determined. Then

$$\nabla\varphi(\boldsymbol{x}, t) + \nabla \times \boldsymbol{\psi}(\boldsymbol{x}, t) = (\Delta g_1(\boldsymbol{x}, t), \Delta g_2(\boldsymbol{x}, t), \Delta g_3(\boldsymbol{x}, t))^{\mathsf{T}}.$$

By inverting the Laplace operator one gets $g_j(\boldsymbol{x}, t) = \Delta^{-1} f_j(\boldsymbol{x}, t)$.

2.2 Fourier operator solution of the scalar wave equation

The general form of a time-dependent Fourier operator A acting on functions $w(\boldsymbol{x})$ of a d-dimensional space variable $\boldsymbol{x}$ is

$$Aw(\boldsymbol{x}, t) = \frac{1}{(2\pi)^d} \iint \mathrm{e}^{i\Phi(\boldsymbol{x}, \boldsymbol{y}, \boldsymbol{\xi}, t)} a(\boldsymbol{x}, \boldsymbol{y}, \boldsymbol{\xi}, t) w(\boldsymbol{y})\, \mathrm{d}\boldsymbol{y}\, \mathrm{d}\boldsymbol{\xi} \tag{2}$$

with a so-called phase function $\Phi(\boldsymbol{x}, \boldsymbol{y}, \boldsymbol{\xi}, t)$ and an amplitude $a(\boldsymbol{x}, \boldsymbol{y}, \boldsymbol{\xi}, t)$. The phase function and the amplitude have to satisfy certain regularity properties so that (2) can be given a meaning as an oscillatory integral, see e.g. [5]. In the cases needed here, the phase function is of the special form $\Phi(\boldsymbol{x}, \boldsymbol{\xi}, t) - \boldsymbol{\xi} \cdot \boldsymbol{y}$ and the amplitude does not depend on $\boldsymbol{y}$. In these cases, the Fourier integral operator can be written in the simpler form

$$Aw(\boldsymbol{x}, t) = \frac{1}{(2\pi)^d} \iint \mathrm{e}^{i\Phi(\boldsymbol{x}, \boldsymbol{\xi}, t) - i\boldsymbol{\xi}\cdot\boldsymbol{y}} a(\boldsymbol{x}, \boldsymbol{\xi}, t) w(\boldsymbol{y})\, \mathrm{d}\boldsymbol{y}\, \mathrm{d}\boldsymbol{\xi} = \frac{1}{(2\pi)^d} \int \mathrm{e}^{i\Phi(\boldsymbol{x}, \boldsymbol{\xi}, t)} a(\boldsymbol{x}, \boldsymbol{\xi}, t) \widehat{w}(\boldsymbol{\xi})\, \mathrm{d}\boldsymbol{\xi} \tag{3}$$

where $\widehat{w}(\boldsymbol{\xi})$ denotes the Fourier transform.

To represent the solution to the scalar wave equation with constant propagation speed (in any space dimension d)

$$u_{tt}(\boldsymbol{x}, t) - c^2 \Delta u(\boldsymbol{x}, t) = f(\boldsymbol{x}, t)$$

by means of Fourier integral operators, it is first decomposed in a decoupled system of *half wave equations*. Setting $v = u_t \mp ic\sqrt{-\Delta}u$ one obtains

$$v_t(\boldsymbol{x}, t) \pm ic\sqrt{-\Delta} v(\boldsymbol{x}, t) = f(\boldsymbol{x}, t).$$

Here $c\sqrt{-\Delta}$ is the pseudodifferential operator with symbol $c|\boldsymbol{\xi}|$. The solution of these half wave equations is given as a sum of Fourier integral operators of the form

$$v(\boldsymbol{x}, t) = \frac{1}{(2\pi)^d} \int \mathrm{e}^{i(\boldsymbol{x}\cdot\boldsymbol{\xi} \mp tc|\boldsymbol{\xi}|)} \left(\hat{v}_0(\boldsymbol{\xi}) + \int_0^t e^{\pm ics|\boldsymbol{\xi}|} \hat{f}(\boldsymbol{\xi}, s) \right) \mathrm{d}\boldsymbol{\xi}$$

where $\hat{f}(\xi, s)$ denotes the Fourier transform with respect to the spatial variables, and v_0 encodes the initial data. This solution is exact. In the general case of non-constant propagation speed one may still construct a so-called parametrix (a solution up to a smooth error) in this way, using Fourier integral operators. However, we shall pursue a more tractable perturbation approach in this paper to deal with non-constant propagation speed.

2.3 Stochastic perturbations

According to the principles laid out in the Introduction, we use a top-down approach. Instead of modelling the randomness through the coefficients of the equations of motion, we solve a deterministic model by means of Fourier integral operators and add parametrized randomness into the solution operator. To construct the perturbed Fourier integral operator, we use the following strategy: Let

$$\frac{1}{(2\pi)^d} \iint \mathrm{e}^{i\Phi(\boldsymbol{x}, \boldsymbol{\xi}, t) - i\boldsymbol{\xi}\cdot\boldsymbol{y}} a(\boldsymbol{x}, \boldsymbol{\xi}) w(\boldsymbol{y}) \mathrm{d}\boldsymbol{y} \mathrm{d}\boldsymbol{\xi}$$

be a term of the solution operator for the wave equation with constant wave speed c_0. Adding random perturbations $r_1(\boldsymbol{x}, \boldsymbol{\xi}, t)$, $r_2(\boldsymbol{x}, \boldsymbol{\xi})$ to the solution operator results in the perturbed, stochastic solution operator

$$\frac{1}{(2\pi)^d} \iint \mathrm{e}^{i(\Phi(\boldsymbol{x}, \boldsymbol{\xi}, t) + r_1(\boldsymbol{x}, \boldsymbol{\xi}, t)) - i\boldsymbol{\xi}\cdot\boldsymbol{y}} (a(\boldsymbol{x}, \boldsymbol{\xi}) + r_2(\boldsymbol{x}, \boldsymbol{\xi})) w(\boldsymbol{y}) \mathrm{d}\boldsymbol{y} \mathrm{d}\boldsymbol{\xi}$$

This representation is very convenient, since one can interpret r_1 as the perturbation geometry of the wave propagation, and r_2 as the perturbation amplitude of the wave number.

In order to guarantee convergence of the perturbed integral, one has to make sure that r_1 and r_2 of the right class, i.e., $\Phi + r_1$ must be a non-degenerate phase function and $a + r_2$ must be of Hörmander symbol class $S^m_{\rho,\delta}$ with $0 < \rho \leq 1, 0 \leq \delta < 1$ (see e.g. [5]). Alternatively, one can take $w(\boldsymbol{y})$ sufficiently smooth and decaying at infinity to arrive at a converging iterated integral.

2.4 Fast Fourier integral operators

The numerical evaluation of the action of a Fourier integral operator is aided by means of the *butterfly algorithm* developed in [6]. A typical term is subjected to a spatial discretization at fixed time t as follows:

$$\iint_{\mathbb{R}^d\times\mathbb{R}^d} \mathrm{e}^{i\Phi(\boldsymbol{x},\boldsymbol{\xi},t)-i\boldsymbol{y}\cdot\boldsymbol{\xi}} w(\boldsymbol{y})\mathrm{d}\boldsymbol{y}\mathrm{d}\boldsymbol{\xi} \approx \Delta_\xi\Delta_y \sum_{k\in\mathcal{G}_\xi} \mathrm{e}^{i\Phi(\boldsymbol{x}_l,\boldsymbol{\xi}_k,t)} \sum_{j\in\mathcal{G}_y} \mathrm{e}^{-i\boldsymbol{y}_j\cdot\boldsymbol{\xi}_k} w(\boldsymbol{y}_j),$$

where $\mathcal{G}_y$ is a spatially discrete and truncated grid in $\mathbb{R}^d$, e.g. $\{\frac{2\pi}{N}(k_1,\dots,k_d)^\mathsf{T}, k_i = 1,\dots,N\}$ and $\mathcal{G}_\xi$ the corresponding grid on the phase side, e.g. $\{(j_1,\dots,j_d)^\mathsf{T}, j_i = 1,\dots,N\}$. Furthermore, Δ_y and Δ_ξ is the volume of a single grid cell in the corresponding discretization. The second sum can be computed by the fast Fourier transform algorithm. So terms of the form

$$\sum_{k\in\mathcal{G}_\xi} \mathrm{e}^{i\Phi(\boldsymbol{x}_l,\boldsymbol{\xi}_k,t)} g(\boldsymbol{\xi}_k)$$

are remaining. A direct evaluation of such a term is very costly and is of complexity $\mathcal{O}((N^d)^2)$. The butterfly algorithm uses a divide and conquer strategy. Thereby the complexity is reduced to $\mathcal{O}((N^d)\log(N))$, which is quite tractable for medium-sized domains and space dimensions $d = 1, 2, 3$.

2.5 A plane strain test model

In order to keep the computational cost low, we use a plane strain problem for the numerical experiments. This refers to a body with infinite extension in z-direction and a driving point force of the form $\boldsymbol{f}(\boldsymbol{x},t) = [\delta(x)\delta(y)\sin(2\pi t), 0, 0]^\mathsf{T}$. By this, $\boldsymbol{u}$ does not depend on z and the displacement is only in (x,y)-direction, i.e., $u_3 \equiv 0$. By that, $g_1(x,y,t) = E(x,y)\sin(2\pi t)$, where $E(x,y) = -(2\pi)^{-1}\log(\sqrt{x^2+y^2})$ is the fundamental solution of the two dimensional Laplace operator, and $\boldsymbol{\Psi} = [0,0,\psi]^\mathsf{T}$ with $\psi = \psi_3$. Thus the problem is reduced to a two-dimensional one, with displacements $u_1(x,y,t)$, $u_2(x,y,t)$. Due to the assumed isotropy of the material, it is no restriction of generality to let the driving force act only in u_2-direction.

After these simplifications, we may assert that there exist a pressure potential Φ and a shear potential Ψ, satisfying the-two dimensional wave equations

$$\begin{aligned} \partial_{tt}\Phi(x,y,t) &= c_l^2\Delta\Phi(x,y,t) - \varphi(x,y,t), \\ \partial_{tt}\Psi(x,y,t) &= c_s^2\Delta\Psi(x,y,t) - \psi(x,y,t), \end{aligned} \tag{4}$$

with

$$\begin{bmatrix} u_1(y,x,t) \\ u_2(x,y,t) \end{bmatrix} = \nabla\Phi(x,y,t) + \begin{bmatrix} -\partial_y\Psi(x,y,t) \\ \partial_x\Psi(x,y,t) \end{bmatrix}. \tag{5}$$

The functions φ and ψ are to be determined by

$$\begin{bmatrix} 0 \\ f(x,y,t) \end{bmatrix} = \nabla\varphi(x,y,t) + \begin{bmatrix} -\partial_y\psi(x,y,t) \\ \partial_x\psi(x,y,t) \end{bmatrix}.$$

The pressure resp. shear wave speed are given by

$$c_l = \sqrt{\frac{(\nu-1)\,E}{(1+\nu)\,(-1+2\,\nu)}}, \qquad \text{resp.} \qquad c_s = \sqrt{\frac{E}{2(\nu+1)}}, \tag{6}$$

where E is the Young modulus and ν is the Poisson ratio. Furthermore, the Dirac point mass $\delta(x)\delta(y)$ is regularized for numerical purposes, the terminal time is set to $T_{\max} = 2$, and thus the actually applied force reads

$$f(x,y,t) = \frac{1}{2\pi\varepsilon^2}\exp\left(-\frac{x^2+y^2}{2\varepsilon^2}\right) f_0(t), \qquad f_0(t) = \sin(2\pi t)\mathbb{1}_{[0,2]}(t),$$

where ε is a small scaling parameter. Since f is a product of a function in time and a function in space, one can see from Section 2.1 that φ and ψ can be represented as

$$\begin{aligned} \varphi(x,y,t) &= \varphi_0(x,y)f_0(t) \\ \psi(x,y,t) &= \psi_0(x,y)f_0(t). \end{aligned}$$

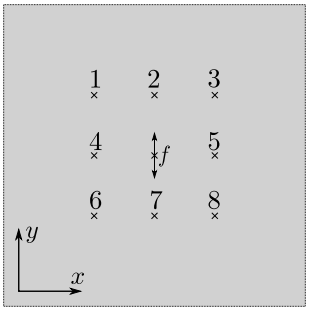

j	x_0	y_0
1	−1.17 cm	−1.17 cm
2	0 cm	−1.17 cm
3	1.17 cm	−1.17 cm
4	−1.17 cm	0 cm
5	1.17 cm	0 cm
6	−1.17 cm	1.17 cm
7	0 cm	1.17 cm
8	1.17 cm	1.17 cm.

Figure 1: The driving force f and the position of the eight (virtual) sensors.

Applying the spatial Fourier transform to equation (4) leads to the ordinary differential equations

$$\partial_{tt}\widehat{\Phi}(\xi,\eta,t) = c_l^2(\xi^2+\eta^2)\widehat{\Phi}(\xi,\eta,t) - \widehat{\varphi}_0(\xi,\eta)f_0(t)$$
$$\partial_{tt}\widehat{\Psi}(\xi,\eta,t) = c_s^2(\xi^2+\eta^2)\widehat{\Psi}(\xi,\eta,t) - \widehat{\psi}_0(\xi,\eta)f_0(t).$$

Solving this and applying the inverse Fourier transform we end up with the following solution operators:

$$\begin{aligned}\Phi(x,y,t) =& \frac{1}{8\pi^2}\int_0^t \left(\int_{\mathbb{R}^2} \mathrm{e}^{ix\xi+iy\eta}\mathrm{e}^{ic_l(t-s)\sqrt{\xi^2+\eta^2}}\widehat{\varphi}_0(\xi,\eta)f_0(s)\,\mathrm{d}(\xi,\eta) \right. \\ &\left. + \int_{\mathbb{R}^2} \mathrm{e}^{ix\xi+iy\eta}\mathrm{e}^{-ic_l(t-s)\sqrt{\xi^2+\eta^2}}\widehat{\varphi}_0(\xi,\eta)f_0(s)\,\mathrm{d}(\xi,\eta) \right) \mathrm{d}s \end{aligned} \tag{7}$$

$$\begin{aligned}\Psi(x,y,t) =& \frac{1}{8\pi^2}\int_0^t \left(\int_{\mathbb{R}^2} \mathrm{e}^{ix\xi+iy\eta}\mathrm{e}^{ic_s(t-s)\sqrt{\xi^2+\eta^2}}\widehat{\psi}_0(\xi,\eta)f_0(s)\,\mathrm{d}(\xi,\eta) \right. \\ &\left. + \int_{\mathbb{R}^2} \mathrm{e}^{ix\xi+iy\eta}\mathrm{e}^{-ic_s(t-s)\sqrt{\xi^2+\eta^2}}\widehat{\psi}_0(\xi,\eta)f_0(s)\,\mathrm{d}(\xi,\eta) \right) \mathrm{d}s. \end{aligned} \tag{8}$$

3 Application to parameter identification and damage detection

For the purpose of demonstration of the method, we use the plane strain model presented is Subsection 2.5. The basic data are specified as follows: The material is assumed to be aluminum with the nominal material parameters $E_{\text{mean}} = 70$ GPa and $\nu_{\text{mean}} = 0.35$. The infinite cuboid is excited by a centered dynamic force acting along the z-axis with frequency 2π MHz. The assumed base domain is 10 cm × 10 cm and $T_{\max} = 7\mu$s. The dimensions of the domain are larger than $c_l \cdot T_{\max}$, thus we do not have to worry about the boundary conditions during the time interval under consideration.

The idea is to calibrate the Fourier integral operator model at data generated by a finite element model, programmed in Abaqus. The numerical Fourier integral operator always has a periodic boundary, whereas the finite element model is equipped with infinite elements at the boundary. The dynamic response is assumed to be measured at eight sensor locations (x_j, y_j), $j = 1 \dots 8$ at all times t, as shown in Figure 1 and the adjacent table.

3.1 Stochastic parameter estimation

In order to get a realistic setting, we assume that the parameters E and ν are randomly perturbed by background random fields R_E, R_ν, assumed to be independent, centered and Gaussian with autocovariance functions

$$\operatorname{cov}\big(R_E(x_1,y_1), R_E(x_2,y_2)\big) = \sigma_E^2\,\mathrm{e}^{-d_{12}/L_E}, \quad \operatorname{cov}\big(R_\nu(x_1,y_1), R_\nu(x_2,y_2)\big) = \sigma_\nu^2\,\mathrm{e}^{-d_{12}/L_\nu} \tag{9}$$

where $d_{12} = \sqrt{(x_1-x_2)^2+(y_1-y_2)^2}$ is the Euclidean distance. Further, σ_E, σ_ν and L_E, L_ν denote the respective standard deviations and correlation lengths. We set $E(x,y) = E_{\text{mean}} + R_E(x,y)$ and $\nu(x,y) = \nu_{\text{mean}} + R_\nu(x,y)$.

The procedure is as follows: The finite element model is fed with a realization of the described random field; the time-dependent output of the FE-simulation is recorded at the eight sensor locations and serves as measured data. The parameters E, ν as well as the stochastic parameters σ_E, σ_ν and L_E, L_ν of the background field are estimated by comparing the data with the solution obtained by the Fourier integral operator representation (5), (7), (8). In Subsection 3.2 the procedure is further extended by adding random terms in the Fourier integral operators in order to get estimators that allow for damage detection (i.e., significant deviations of the material properties).

3.1.1 Estimating the nominal values

The first task is to estimate the nominal values $E_0 = E_{\text{mean}}$ and $\nu_0 = \nu_{\text{mean}}$ based on the data given in the sensor locations. One expects that the estimator for E_0 and ν_0 varies more, if the variances of the random fields in the FE-model increase. It may also depend on the correlation lengths. This is about to be examined in the following.

To shorten notation, we let $\boldsymbol{g}_j(t) = \boldsymbol{u}_{\text{FEM}}(x_j, y_j, t)$ be the solution given by the FEM simulation with the given realization of the random field at sensor location (x_j, y_j), recorded over the time interval $[0, T_{\max}]$. Thus $\boldsymbol{g} = [g_{d,j}], d = 1, 2$ is a matrix-valued function. The FIO solution $\boldsymbol{h}_j(t, E_0, \nu_0) = \boldsymbol{u}_{\text{FIO}}(x_j, y_j, t, E_0, \nu_0)$, solves the deterministic, constant coefficient case with parameters E_0 and ν_0, and $\boldsymbol{h} = [h_{d,j}], d = 1, 2$.

Goodness of fit is measured in terms of the norm

$$\|\boldsymbol{f}\|_{2,1} := \sum_{j=1}^{8} \|\boldsymbol{f}_j\|_2 := \sum_{j=1}^{8} \sqrt{\sum_{d=1}^{2} w_d \int_0^{T_{\max}} f_{d,j}^2(t)\,\mathrm{d}t},$$

for fixed weights w_d, and E_0, ν_0 are estimated as solutions to the minimization problem

$$[E_{0,\text{opt}}, \nu_{0,\text{opt}}] = \operatorname*{argmin}_{E_0,\nu_0} \|\boldsymbol{g} - \boldsymbol{h}(\cdot, E_0, \nu_0)\|_{2,1}\,.$$

For the minimization problem we used the standard Nelder-Mead simplex algorithm. If $\sigma_E = 0$, the algorithm converges to the true value, even if one chooses a bad starting value. For $\sigma_E > 0$ it turned out that the algorithm is very robust, and still converges almost to the true value after at most 15 iterations.

If E and ν are stochastically perturbed, one can increase the robustness of the algorithm by repeating the FE-computation with N different realizations of the random fields and estimating E_0 and ν_0 by the corresponding sequence of $E_{0,\text{opt}}^{(1)}, \ldots, E_{0,\text{opt}}^{(N)}$ and $\nu_{0,\text{opt}}^{(1)}, \ldots, \nu_{0,\text{opt}}^{(N)}$ and setting:

$$E_0 \approx \widehat{E}_0 = \frac{1}{N}\sum_{k=1}^{N} E_{0,\text{opt}}^{(k)}, \qquad \nu_0 \approx \widehat{\nu}_0 = \frac{1}{N}\sum_{k=1}^{N} \nu_{0,\text{opt}}^{(k)}.$$

A sample size of $N < 10$, say, gives already a robust estimate.

3.1.2 Estimating the stochastic parameters

Our next task is to estimate σ_E^2 and σ_ν^2. It turned out to be favorable to estimate the parameters for each sensor. Accordingly, we get for sensor j:

$$[E_{0,\text{opt},j}, \nu_{0,\text{opt},j}] = \operatorname*{argmin}_{E_0,\nu_0} \|\boldsymbol{g}_j(\cdot) - \boldsymbol{h}_j(\cdot, E_0, \nu_0)\|_2\,.$$

Computing the Poisson ratio numerical experiments showed that

$$\widehat{\sigma}_\nu^2 = \sigma_{\nu_{0,\text{opt}}}^2 = \text{var}(\nu_{0,\text{opt}})$$

gives a good estimate for σ_ν^2, where $\sigma_{\nu_{0,\text{opt}}}^2$ is estimated by

$$\sigma_{\nu_{0,\text{opt}}}^2 = \frac{1}{8N-1}\sum_{j=1}^{8}\sum_{k=1}^{N}\left(\nu_{0,\text{opt},j}^{(k)} - \widehat{\nu}_0\right)^2.$$

A sample size of $N = 100$ is recommendable. However, for Young's modulus the analogous estimate turned out to fail:

$$\sigma_E^2 \not\approx \sigma_{E_{0,\text{opt}}}^2 = \text{var}(E_{0,\text{opt}}),$$

with

$$\sigma_{E_{0,\text{opt}}}^2 = \frac{1}{8N-1}\sum_{j=1}^{8}\sum_{k=1}^{N}\left(E_{0,\text{opt},j}^{(k)} - \widehat{E}_0\right)^2. \tag{10}$$

The solution we adopted was to obtain a correction term empirically by Monte Carlo simulation. We examine the connection between $\sigma_{E_{0,\text{opt}}}$ on the one hand and σ_E and L_E on the other hand. Figure 2

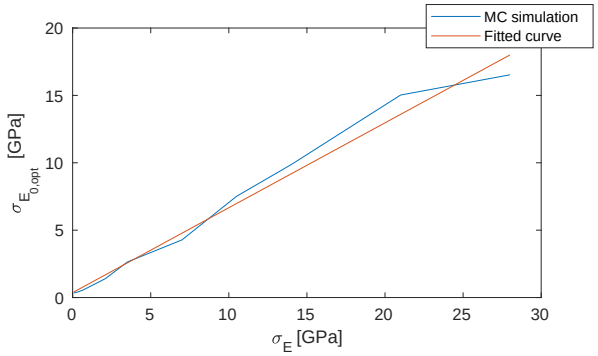

Figure 2: Dependence of $\sigma_{E_{0,\mathrm{opt}}}$ on σ_E with fixed correlation length $L = 3$ cm.

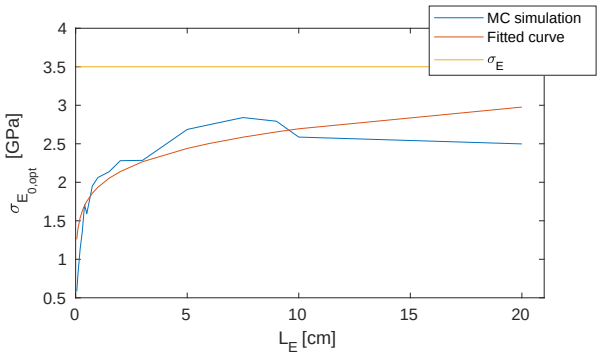

Figure 3: Dependence of $\sigma_{E_{0,\mathrm{opt}}}$ on L_E for fixed $\sigma_E = 0.05 \cdot E_0$.

shows the dependence of $\sigma^2_{E_{0,\mathrm{opt}}}$ and σ^2_E for a fixed L_E. One can clearly observe a linear dependence. The calculation was done with a sample size of $N = 100$ for each σ_E from the list

$$\{0.001, 0.005, 0.01, 0.03, 0.05, 0.10, 0.15, 0.20, 0.30, 0.40\} \cdot 70 \ \text{ GPa}.$$

Figure 3 shows the dependence of $\sigma^2_{E_{0,\mathrm{opt}}}$ and L_E for a fixed σ^2_E. This graph was used to fit a function $\mathfrak{f}(L_E)$. Combining this with the linear dependence of $\sigma^2_{E_{0,\mathrm{opt}}}$ on σ^2_E at fixed L_E, we arrive at the functional relation $\sigma_{E_{0,\mathrm{opt}}} = \sigma_E\, \mathfrak{f}(L_E)$, and so for a given L_E we can estimate

$$\widehat{\sigma}_E = \sigma_{E_{0,\mathrm{opt}}} / \mathfrak{f}(L_E). \tag{11}$$

Thus it remains to estimate the correlation length L_E. Since we have different sensor locations, one can also estimate the correlation between the sensors and from there the correlation length. We assume that the parameters in the sensor locations derive from a stationary random field obeying the covariance function

$$\mathrm{cov}(E_{0,\mathrm{opt},j_1}, E_{0,\mathrm{opt},j_2}) = C(r) = \sigma^2_{E_{0,\mathrm{opt}}} \exp\left(-\frac{r}{L_{E_{0,\mathrm{opt}}}}\right), \tag{12}$$

where $r = \sqrt{(x_{j_1} - x_{j_2})^2 + (y_{j_1} - y_{j_2})^2}$. We pair the sensors as shown in Table 1 and estimate

$$C(r_i) \approx \frac{1}{N\,|\mathcal{P}_i| - 1} \sum_{k=1}^{N} \sum_{[j_1,j_2]\in\mathcal{P}_i} \left(E^{(k)}_{0,\mathrm{opt},j_1} - \widehat{E}_{0,j_1}\right)\left(E^{(k)}_{0,\mathrm{opt},j_2} - \widehat{E}_{0,j_2}\right).$$

By fitting the empirical covariances to the autocovariance function, one gets an estimator for $L_{E_{0,\mathrm{opt}}}$. Figure 4 shows the results of a Monte Carlo simulation with $N = 100$ for each L_E from

$$\{0.05, 0.1, 0.2, 0.3, 0.4, 0.5, 0.75, 1, 1.5, 2, 3, 5, 6, 7.5, 9, 10, 20\} \ \text{ cm},$$

as well as the fitted scaling curve, resulting in a relation

$$L_E = \mathfrak{g}\big(L_{E_{0,\mathrm{opt}}}\big). \tag{13}$$

To summarize, in order to estimate σ_E and L_E, one starts by computing $\sigma_{E_{0,\mathrm{opt}}}$ from (10). Then the empirical correlation length $L_{E_{0,\mathrm{opt}}}$ is evaluated by fitting model (12) to the sensor data. Next, L_E is estimated using the empirical relation (13), and finally σ_E is obtained from the relation (11).

Table 1: Pairing of sensors and corresponding distances.

Sensor pairs ($\mathcal{P}$)					
$\mathcal{P}_0$	$\mathcal{P}_1$	$\mathcal{P}_2$	$\mathcal{P}_3$	$\mathcal{P}_4$	$\mathcal{P}_5$
$[1,1]$	$[1,2]$	$[2,4]$	$[1,3]$	$[1,5]$	$[1,8]$
$[2,2]$	$[1,4]$	$[2,5]$	$[1,6]$	$[1,7]$	$[3,6]$
$[3,3]$	$[2,3]$	$[4,7]$	$[3,8]$	$[2,6]$	
$[4,4]$	$[3,5]$	$[5,7]$	$[6,8]$	$[2,8]$	
$[5,5]$	$[4,6]$			$[3,4]$	
$[6,6]$	$[5,8]$			$[3,7]$	
$[7,7]$	$[6,7]$			$[4,8]$	
$[8,8]$	$[7,8]$			$[5,6]$	

Distance between sensors (r)					
r_0	r_1	r_2	r_3	r_4	r_5
0 cm	1.17 cm	1.65 cm	2.34 cm	2.62 cm	3.31 cm

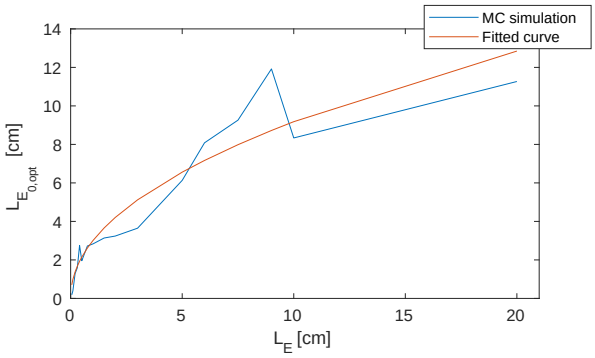

Figure 4: Dependence of $L_{E_{0,\mathrm{opt}}}$ on L_E, simulation and fitted scaling curve.

3.2 Testing for damage

This subsection is dedicated to devising statistical tests, indicating whether the properties of a given material are within certain bounds or not. The strategy is as follows. One generates a sample of signals in the sensor locations by means of stochastic Fourier integral operators. If the measured signal is not too different from the Monte Carlo sample, the material is considered "good". The generation of the Monte Carlo sample can be done in advance of the testing.

To generate the sample we perturb the deterministic phase functions of the solution FIOs (see (7), (8))

$$\varphi_w(x,y,\xi,\eta,s,t) = x\xi + y\eta + ic_w^2(t-s)\sqrt{\xi^2+\eta^2}, \qquad w = l,s$$

by making c_l and c_s space dependent and setting

$$c_l(x,y) = \sqrt{\frac{(\nu(x,y)-1)\,E(x,y)}{(1+\nu(x,y))\,(-1+2\,\nu(x,y))}}, \qquad \text{resp.} \qquad c_s(x,y) = \sqrt{\frac{E(x,y)}{2(\nu(x,y)+1)}}, \tag{14}$$

that is, we replace the constant parameters E and ν from formula (6) by random fields

$$E(x,y) = E_{\mathrm{mean}} + R_E(x,y), \qquad \nu(x,y) = \nu_{\mathrm{mean}} + R_\nu(x,y).$$

Here R_E and R_ν are Gaussian random fields of the form (9) with parameters corresponding to the undamaged state (the null hypothesis described below).

Since for engineering purposes usually the Young's modulus is the critical factor we focus on detecting changes in E_{mean} or σ_E.

The parameter values for the undamaged state were assumed to be $E_{\mathrm{mean}} = 70$ GPa and $\nu = 0.35$; slight variations were admitted following background random fields with $\sigma_E = 3.5$ GPa, $\sigma_\nu = 0.005$ and $L_E = L_\nu = 3$ cm. These were the data entered in the FE-model as well as the wave speeds of the FIOs according to (14). In practice, estimated values would be entered in (14) according to Subsection 3.1.

The coefficients of variations were so small that no problems with the square roots in (14) could arise, and further cut-offs were not needed.

The null hypothesis was that the material is in the undamaged state, i.e., it has the parameters described above. The first step was to generate a sample of size $N = 1000$ of system responses, distributed according to the null hypothesis, by means of the FIO-solution operator with wave speeds (14). The null hypotheses is tested against FE-output generated with perturbed parameters or with inclusion of a crack.

In order to test the material one has to choose characteristic features of the signal. This choice is very critical, since a bad set of features can lead to a poor distinction between good and bad material. In our case it turned out that the total spectral energy of the signal, the phase angle and the spectral energy density of selected frequencies are working well enough. In fact, we had eight sensor locations with signals in x- and y-direction. The four signals in x-direction at sensors 2, 4, 5, 7 were close to zero. (Due to the special excitation, no shear waves arrive at sensors 4 and 5, and no pressure waves arrive at sensors 2 and 7.) Thus 12 signals remained for the analysis. Of each signal 5 features were extracted: the total spectral energy density and the phase angle and spectral energy density at the first two nonzero frequencies in the DFT-spectrum (in our case $\omega_1 = 2\pi/7 \approx 0.9$ MHz and $\omega_2 = 4\pi/7 \approx 1.8$ MHz). Thus a total number of 60 features was used for damage detection.

In principle, a significance test works as follows. One first chooses a significance level α, say 1% or 5% and computes the $(1-\alpha)$-confidence interval of the feature under consideration from the sample as generated above. The null hypotheses is rejected if the measured value lies outside the confidence interval. In our situation such a test can be tuned in several ways:

(a) Choice of significance level α. A small α means that rejection is more affirmative, while acceptance is easier.

(b) Decision about the number of signals leading to rejection or acceptance (out of the 60 available features).

(c) The overall choice of features taken into account.

Further, one could also use the p-values and a possible ranking of them in place of the test based on confidence intervals. In addition, a bias due to a possible modeling difference in the sample and the measurement may arise. In our case, the amplitude of the FIO-signal was systematically too small, because reflected waves could arise in the FE-model, but not in the FIO-representation. Notwithstanding these words of caution, we present the results of several scenarios, using a significance level of $\alpha = 1\%$, hence 99%-confidence intervals and a sample of FIO-solutions computed with the parameters of the undamaged state described above.

(1) Scenario 1: The material is having the desired properties (undamaged state).

(2) Scenario 2: The material is not having the desired properties: E_{mean} is too small (60 MPa).

(3) Scenario 3: The material is not having the desired properties: E_{mean} is too large (80 MPa).

(4) Scenario 4: The material is having the desired properties, but is suffering a crack. The crack is modeled by a small region in the FE-model having a very small Young's modulus.

Figure 5 shows realizations of the random field $E(x, y)$ in Scenarios 1–4. As mentioned, the confidence bounds for the null hypotheses were generated by a sample of size 1000 simulated stochastic FIO solutions. Using a 99%-confidence interval in all scenarios, the following results were obtained in repeated test trials:

(1) Scenario 1: The null hypothesis is not rejected. In most of all trials, all of the 60 features accepted the null hypothesis. In some trials, acceptance happened in slightly fewer, but well above 55 features. This would also have been the case, had we used the more strict 95%-interval.

(2) Scenario 2: The null hypothesis is rejected in almost all sensor locations. Since E_0 is small, the signal arrives late, and the phase angle is out of the 99%-interval.

(3) Scenario 3: The null hypothesis is rejected in almost all sensor locations. Since E_0 is large, the signal arrives early, and the phase angle is out of the 99%-interval.

(4) Scenario 4: Since the crack lies between sensor 3 and the origin, the pulse changes. Thus the sensor in location 3 diagnoses the damage by rejecting the null hypothesis due to a large spectral energy, in total and at both frequencies ω_1 and ω_2, while the others do not. Since there is only one sensor location rejecting the null hypothesis, one can interpret this as the detection of the crack location.

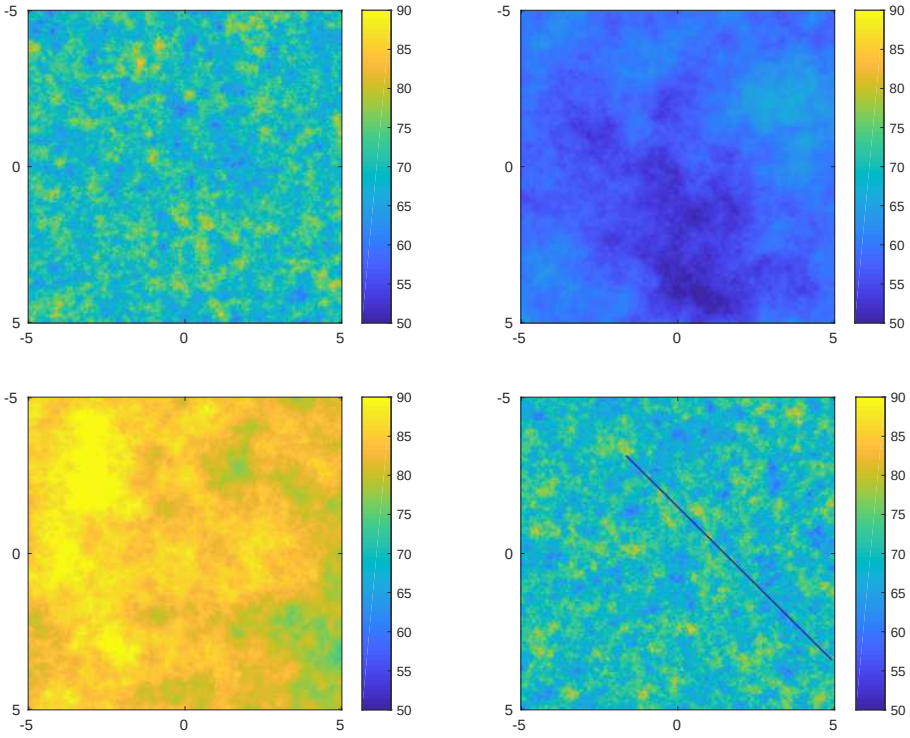

Figure 5: Realizations of the random field $E(x, y)$ (Young's modulus) in Scenarios 1–4. From upper left to lower right: Scenario 1 (undamaged), Scenario 2 (E_{mean} is too small), Scenario 3 (E_{mean} is too large), Scenario 4 (crack).

Exemplarily, we show the graphical analysis for Scenarios 1 and 4 in Figures 6 and 7. The upper parts of the figures show the temporal evolution of the FEM-signal (red line) and of the whole Monte Carlo sample (shaded region) in sensor location 3. The histograms show the 99% confidence interval (black lines) and the value of the measured signal (red line), referring to the phase angle and the spectral energy density at frequency $\omega_2 = 1.8$ MHz, and the total spectral energy density (displacement in x-direction).

In our trial cases, the method was capable of arriving at the correct diagnosis in all four scenarios. Further trial cases aiming at the detection of changes in σ_E were successfully undertaken as well. As a final remark, let us note that Gaussian random fields were used for the sake of demonstration. This has the advantage that the statistical properties of Gaussian random fields are fully controlled by their second moments, both in calibration and simulation. The strategy outlined here may be used with non-Gaussian random fields as well, should the data suggest it.

4 Summary

In this article, a new method for analyzing wave propagation in random media using records of the time dependent response of a dynamically excited structure has been presented. The method is based on the Fourier integral operator representation of the solution to the equations of motion of a linear elastic material. It has been demonstrated by means of data generated by a finite element model that the material parameters can be identified by fitting the solution computed through the Fourier integral operator representation. Random perturbations have been incorporated as additive terms in the phase functions of the Fourier integral operators. In this way, confidence intervals around the nominal response of the unperturbed structure can be calculated. This allows one to detect fatigue or damage in the material through hypothesis tests with the signals of the damaged structure. The intended goals of parameter identification and damage detection have been attained in benchmark examples.

The models can be implemented in real case applications after suitable adaptations. While in the paper, a two-dimensional problem has been addressed, the method is applicable in any space dimension. In the fully three-dimensional case, high computing power is required. A further topic of research could be to reduce the computational cost in the three-dimensional case. The computational cost in the one- and two-dimensional case is low enough to be performed on a standard computing equipment.

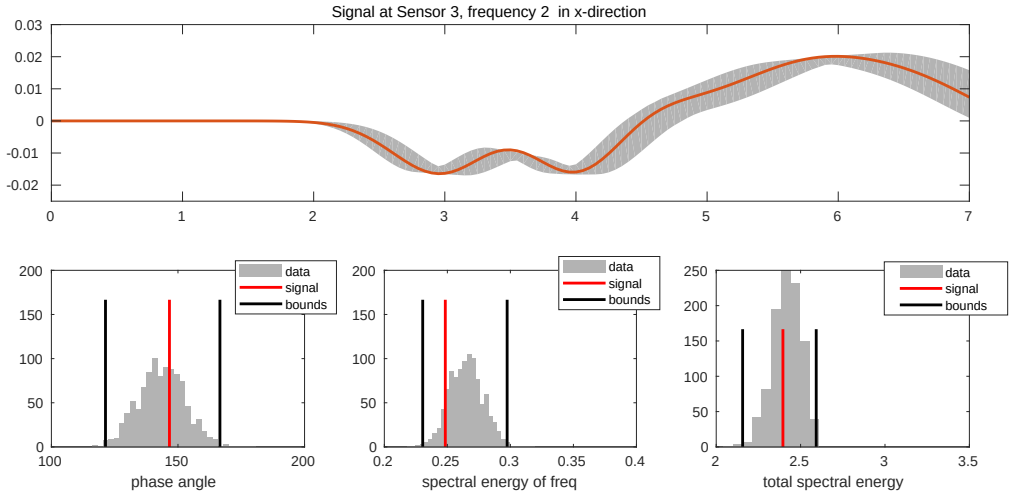

Figure 6: Comparison of signal (displacement in x-direction) and Monte Carlo sample in sensor location 3, showing acceptance of the null hypothesis at the 99% confidence level (Scenario 1, undamaged material).

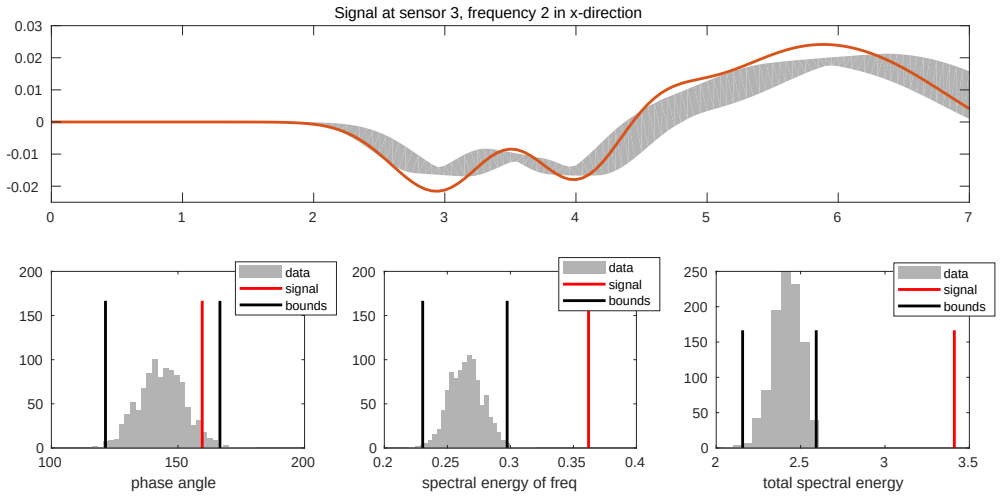

Figure 7: Comparison of signal (displacement in x-direction) and Monte Carlo sample in sensor location 3, showing rejection of the null hypothesis at the 99% confidence level (Scenario 4, crack).

Acknowledgments

We thank our industrial partners INTALES Engineering Solutions, Natters, Austria, for important input and advice on the project. We gratefully acknowledge support by The Austrian Research Promotion Agency (FFG) in the framework of the Bridge Program, Project No. 4602529.

References

[1] M. Oberguggenberger and M. Schwarz, Fourier integral operators in stochastic structural analysis, in *Proceedings of the 12th International Probabilistic Workshop*, edited by F. Werner, M. Huber, T. Lahmer, T. Most, and D. Proske (Bauhaus-Universitätsverlag, Weimar, 2014), 250–257.

[2] L. Lamplmayr, M. Oberguggenberger, and M. Schwarz, Stochastic Fourier integral operators for damage detection, in *A Proc. of the 15th Inter. Prob. W. & 10th Dresdner Prob. W.*, edited by M. Voigt, D. Proske, W. Graf, M. Beer, U. Häußler-Combe, and P. Voigt (Dresden, 2017), 73–84.

[3] K. Graff, *Wave Motion in Elastic Solids* (Clarendon Press, Oxford, 1975).

[4] V. Poruchikov, *Methods of the Classical Theory of Elastodynamics* (Springer, Berlin, 1993).

[5] M. Shubin, *Pseudodifferential Operators and Spectral Theory* (Springer, Berlin, 2001).

[6] E. Candès, L. Demanet, and L. Ying, A fast butterfly algorithm for the computation of Fourier integral operators, *Multiscale Modeling & Simulation* **7**, 1727 (2009).